Journal of Porphyrins and Phthalocyanines
J. Porphyrins Phthalocyanines 2021; **25**: 756–771
DOI: 10.1142/S1088424621500826

Published at https://www.worldscinet.com/jpp/

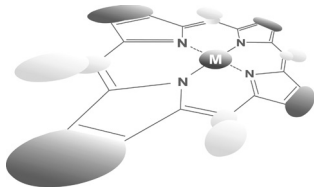

A new inhibition mechanism in the multifunctional catalytic hemoglobin dehaloperoxidase as revealed by the DHP A(V59W) mutant: A spectroscopic and crystallographic study

Matthew K. Thompson[a]*, Madeline R. Shay[a], Vesna de Serrano[b], Rania Dumarieh[b], Reza A. Ghiladi[b◊] and Stefan Franzen[b]

[a]*Department of Chemistry & Biochemistry, University of Alabama, 250 Hackberry Lane, Tuscaloosa, AL 35487, USA*
[b]*Department of Chemistry, North Carolina State University, Raleigh, NC 27695, USA*

Received 1 May 2021
Accepted 14 June 2021

Dedicated to Professor Jonathan S. Lindsey on the occasion of his 65th birthday

ABSTRACT: As multifunctional catalytic hemoglobins, dehaloperoxidase isoenzymes A and B (DHP A and B) are among the most versatile hemoproteins in terms of activities displayed. The ability of DHP to bind over twenty different substrates in the distal pocket might appear to resemble the promiscuousness of monooxygenase enzymes, yet there are identifiable substrate-specific interactions that can steer the type of oxidation (O-atom *vs*. electron transfer) that occurs inside the DHP distal pocket. Here, we have investigated the DHP A(V59W) mutant in order to probe the limits of conformational flexibility in the distal pocket as it relates to the genesis of this substrate-dependent activity differentiation. The X-ray crystal structure of the metaquo DHP A(V59W) mutant (PDB 3K3U) and the V59W mutant in complex with fluoride [denoted as DHP A(V59W-F)] (PDB 7MNH) show significant mobility of the tryptophan in the distal pocket, with two parallel conformations having W59-$N^{\varepsilon 1}$ H-bonded to a heme-bound ligand (H_2O or F^-), and another conformation [observed only in DHP A(V59W-F)] that brings W59 sufficiently close to the heme as to preclude axial ligand binding. UV-vis and resonance Raman spectroscopic studies show that DHP A(V59W) is 5-coordinate high spin (5cHS) at pH 5 and 6-coordinate high spin (6cHS) at pH 7, whereas DHP A(V59W-F) is 6cHS from pH 5 to 7. Enzyme assays confirm robust peroxidase activity at pH 5, but complete loss of activity at pH 7. We find no evidence that tryptophan plays a role in the oxidation mechanism (*i.e*. radical formation). Instead, the data reveal a new mechanism of DHP inhibition, namely a shift towards a non-reactive form by OH^- ligation to the heme-Fe that is strongly stabilized (presumably through H-bonding interactions) by the presence of W59 in the distal cavity.

KEYWORDS: Peroxidase, hemoglobin, structure-function, tryptophan, inhibition.

INTRODUCTION

The protein structure-function correlation has been built from decades of study of primarily monofunctional systems, but whether (and how) structure uniquely defines function in multifunctional systems is a significantly more complex subject to address. This complexity is easily seen within the heme protein superfamily, where functions as diverse as reversible O_2-transport, enzymatic activity (*i.e*. peroxidase, peroxygenase, oxygenase, and oxidase) and electron-transfer all occur at active sites that are often remarkably similar in terms of both structure and mechanism, but where the protein environment exquisitely controls the chemical reactivity of the

[◊] SPP full member in good standing.

Correspondence to: Matthew K. Thompson. email: mthompson 10@ua.edu — tel.: (205) 348-7020.

heme group to ensure maximum intended function with a minimum of unintended cross reactivity. Understanding how Nature controls functional selectivity ("activity differentiation") across the heme protein superfamily has been a longstanding question that penetrates to the core of the protein structure-function correlation. Despite decades of study, it remains a challenge to fully understand the factors in a multifunctional system that influence a reactive heme intermediate between, as just one example, peroxygenase (oxygen atom transfer) [1] and peroxidase (electron transfer) [2] activities.

Our chosen platform for probing the structural and mechanistic considerations that lead to activity differentiation in multifunctional heme proteins is the enzyme dehaloperoxidase (DHP). This coelomic hemoglobin from the marine worm *Amphitrite ornata* has shown a broad range of mechanistic functions: beyond its role as an oxygen transport protein, DHP possesses four enzymatic activities necessary for the survival of *A. ornata* (peroxidase, peroxygenase, oxidase and oxygenase), all of which employ a common Fe(IV)-oxo intermediate. This diversity of oxidative function displayed by DHP permits degradation of a variety pollutants (*i.e.* naturally-occurring brominated phenols, indoles and pyrroles found in coastal estuaries and mud flats within which *A. ornata* inhabits [3–5]), perhaps not optimally, but with sufficient activity to prevent the most harmful effects. Initially, it appeared that understanding the non-standard peroxidase reaction was the challenge [6], however further research definitively revealed both high and specific reactivity towards brominated (and other halogenated) substrates [7–10]. First, 4-halophenols [11–14] and then 2,4,6-trihalophenols [15–17] were shown to bind inside the distal pocket of DHP A. A high-pressure xenon X-ray crystal structure revealed an ideal binding site for a large halogen atom, *e.g*. bromine, deep within the protein [18]. Studies employing DHP isoenzyme B [19] have revealed the range of small molecules capable of binding inside the distal pocket, including azoles [20], guaiacols [21], cresols [22], nitrophenols [23], catechols [23], bromoindoles [8] and pyrroles [10]. Within the wealth of the ~40 DHP-ligand structures above are different binding geometries that have functional consequence, specifically it appears that different substrates are oxidized by different mechanisms, which may depend on the shape or electrostatics of the substrate that binds within the distal pocket [9, 21, 24].

Although steric effects are often easier to predict, a protein as flexible as DHP begs the question, how much space really exists in the distal pocket for substrate binding? Numerous studies have addressed how the shape (or electronic properties) of the distal pocket will influence the reactivity of DHP [6, 7, 13, 14, 25–29]. Surface electrostatic mutants (amino acid swaps that differ by a charge) have shown that the barrier for the binding of TCP to DHP is strongly controlled by electrostatics [27]. Closer to the heme cofactor, it is not an accident that much emphasis has been placed on the distal histidine, H55, as the locus of function switching given the role of this residue in activating H_2O_2 in the Poulos-Kraut mechanism [30]: H55 has been mutated to several other side chains, including H55V, H55A, and H55D [31]. Immediately adjacent to H55 is the T56 site, and mutants in this location (*i.e*. T56S, T56V, T56A) had predictable effects on either locking the histidine in place (such as occurs in most heme proteins, T56V) or permitting a greater freedom of motion (T56A). Interestingly, efforts to sterically interfere with DHP function have shown varied success, including L100F in DHP A [14], the F21W mutant of both isoenzymes [9, 16] and a wide variety of tyrosine mutants [32]. As one example, we have previously demonstrated that the F21W variant leads to a more than 7-fold attenuation in catalytic efficiency for its peroxidase activity when employing 2,4,6-trichlorophenol (TCP) as the substrate, but minimal decreases in peroxygenase activity (<2-fold) as measured by 4-nitrophenol or 5-Br-indole substrate conversion [9]. Structural studies of DHP B(F21W) (PDB 5VLX) have shown that the tryptophan residue overlaps significantly with one of the two identified TCP binding sites ($TCP_{interior}$), leaving the other site ($TCP_{exterior}$) available for binding peroxygenase substrates, and suggests that it is possible to selectively tune the of activity of a multifunctional enzyme through judicious introduction of steric bulk.

Given the above results afforded by the DHP B(F21W) mutant, it is of particular interest to see if there are any levers or switches available with regard to activity differentiation that reveal themselves in a more congested structure near the vicinity of the active site heme iron. In this regard, the distal valine, V68, in SWMb has the unique distinction of being the closest distal amino acid to the heme Fe [33]. In globins, V68 is a "gate-keeper" for the heme iron, playing a role in directing the binding of oxygen in hemoglobin and myoglobin [34–37], but also azide and cyanide in metmyoglobin [38]. Mutations of V68 have been particularly informative: in studies of ligand trajectories (*e.g.* binding of NO and kinetics of NO recombination in SWMb and human Mb), tryptophan mutations have played a key role in blocking certain entrance and exit channels [39–41]. Guided by these precedents for V68 mutants in myoglobin, in this study we have chosen to similarly introduce a tryptophan at the analogous distal valine, V59, in dehaloperoxidase-hemoglobin A (DHP A) in order to further understand the steric effects in the open distal pocket. The present study provides evidence that amino acid side chains can interact with bound heme-Fe ligands (H_2O, OH^-, F^-) in the ferric form. As will be shown from a combination of structural and spectroscopic studies, the observation for DHP A(V59W) is that the steric bulk of the tryptophan side chain has a minimal effect on enzyme kinetics at pH < 7, but at pH > 7 the tryptophan can sufficiently stabilize a six coordinate Fe-OH adduct such that the enzyme loses catalytic activity. These results have implications

for the rational design of mutants employing bulky amino acids to tune the activity of multifunctional heme enzymes, such as DHP, which have flexible active sites that can accommodate a wide variety of substrates, possibly even without the requirement that the distal histidine be positioned to serve as the general acid/base catalyst of the Poulos–Kraut [30] mechanism (as was found for the F21W mutant of DHP B [9]). Interestingly, DHP itself has been shown to oxidize 10 out of the 11 phenolic compounds on the EPA Priority Pollutants list [22, 25], demonstrating the potential of this multifunctional enzyme as a promising biocatalyst for bioremediation applications as was first suggested by Lebioda and coworkers [11]. More broadly, given that DHP is capable of five major activities associated with heme proteins within a single active site, these studies on a multifunctional enzyme can advance our understanding of the structure-function correlation beyond what has been built from decades of study of monofunctional proteins, and furthers our ability to provide comparisons of the structure–function correlation in marine enzymes to those of terrestrial or bacterial origins.

METHODS

Materials — Buffer salts were purchased from Fisher Scientific. Crystallization grade potassium fluoride was from Hampton Research. All other reagents and biochemicals, unless otherwise specified, were of the highest grade available from Sigma Aldrich. Solutions of 100 mM potassium phosphate monobasic and 100 mM potassium phosphate dibasic were prepared initially. These two solutions were then combined in appropriate proportions in order to make 100 mM potassium phosphate buffer solutions at three different pH values, pH 5, 6, and 7. Solutions of trihalogenated phenols were freshly prepared prior to each experiment in 100 mM potassium phosphate (KP_i) buffer at the appropriate pH and kept at 4 °C in the dark until used. UV-vis spectra were recorded periodically to ensure that the co-substrate had not degraded by monitoring its absorbance: trifluorophenol, 270 nm (1027 M^{-1} cm^{-1}); trichlorophenol, 312 nm (3752 M^{-1} cm^{-1}); tribromophenol, 316 nm (5055 M^{-1} cm^{-1}) [42]. Hydrogen peroxide stock solutions were also freshly prepared daily prior to each experiment and maintained at 4 °C. The hydrogen peroxide stability was monitored by UV-vis spectroscopic analysis at 240 nm (ε_{240} = 43.6 M^{-1} cm^{-1}) [43]. The stock H_2O_2 solution was diluted to the corresponding premixing concentrations for each experiment.

Mutagenesis and protein preparation. The V59W point mutation was introduced into the 6XHisDHPA4R gene [44] using the QuikChange II Site-Directed Mutagenesis kit (Stratagene, La Jolla, CA), and the desired mutation and lack of deleterious secondary ones were confirmed by sequencing. The pET 16b plasmid containing the 6XHisDHPA4R or 6XHisDHPA4R V59W DNA insert was transformed into BL21 (DE3) *Escherichia coli* cells and plated out on 2xYT/Ampicillin agar plates. Single colonies were isolated and overnight cultures were scaled up to 6 L growths. Expression of 6XHisDHP A protein was not induced *via* addition of ITPG. After subsequent cell harvesting and lysis, the His-tagged protein was isolated using immobilized metal affinity chromatography using Ni-NTA agarose (Qiagen), followed by further purification *via* ion exchange chromatography (CM 52) as discussed elsewhere [44]. Purified DHP A was dialyzed in 0.1 M potassium phosphate buffer at pH 7 and oxidized using $K_3Fe(CN)_6$. Excess $K_3Fe(CN)_6$ was subsequently removed using a 20 cm X 1 cm hand packed Sephadex G-25 column. DHP concentration was determined using the Soret band at 406 nm with a molar absorptivity of 116,400 M^{-1} cm^{-1} for metaquo DHP A [45].

UV-vis spectroscopic studies of DHP A(V59W) — DHP A(V59W) was treated with an excess of potassium ferricyanide in order to obtain a homogeneous solution of the enzyme in the ferric state. Ferri/ferrocyanide was removed using a PD-10 desalting column prepacked with Sephadex G-25 medium. The protein was concentrated using an Amicon Ultra centrifugal filter equipped with a 10 kDa cutoff molecular weight membrane, and the purity of DHP A was determined as previously published [42]. The molar absorptivity for DHP A (ε_{406} = 116.4 $mM^{-1}cm^{-1}$) [45] was used as the basis for that of DHP A(V59W). Optical spectra were recorded using quartz microcuvettes (1 cm pathlength) on a Cary 50 UV-vis spectrophotometer equipped with thermostatted cell holders at 25 °C or on an Agilent 8453 UV-vis spectrometer running ChemStation software. Solutions of ferric DHP A (10 μM final concentration) were prepared in 100 mM KP_i buffer at pH 5, 6, and 7.

Dehaloperoxidase activity assays — Optical spectra were recorded using quartz microcuvettes (1 cm pathlength) as described above. The apparent value of k_{cat} for DHP A(V59W) was calculated by method of initial rates, and the experimental data were fitted to the Michaelis-Menten model using the enzyme kinetics software GraFit (Erithacus Software). The enzymatic activity was assayed on the basis of the formation of dichloroquinone product (275 nm) [ε_{275} = 11,400 $M^{-1}cm^{-1}$ for TCP] monitored for 5 min at 25 °C. The 1-mL reaction mixture contained 10 μM of enzyme (ferric) and 300 μM of trichlorophenol in 100 mM potassium phosphate buffer at pH 6, and was initiated upon addition of 100 μM H_2O_2.

Stopped-flow UV-vis spectroscopic studies. Optical spectra were recorded using a Bio-Logic SFM-400 triple-mixing stopped flow instrument coupled to a rapid scanning diode array UV-visible spectrophotometer. The temperature was maintained at 25 °C with a circulating water bath, and all solutions were prepared in 100 mM KP_i (pH 7). Experiments were performed in single-mixing mode where DHP A(V59W) at a final concentration of 10 μM was reacted with 2.5–25 equivalents of H_2O_2.

Control experiments were performed in the absence of hydrogen peroxide. Data were collected (900 scans total) over a three-time domain regime (2.5, 25, and 250 ms; 300 scans each) using the Bio Kinet32 software package (Bio-Logic). All data were evaluated using the Specfit Global Analysis System software package (Spectrum Software Associates) and fit to exponential functions as one-step/two-species, two-step/three species, or three-step/four species irreversible mechanisms where applicable. Data were baseline corrected using the Specfit autozero function.

Rapid freeze-quench EPR spectroscopic studies of H_2O_2-activated DHP A(V59W). A BioLogic SFM 400 Freeze-Quench apparatus was used to prepare samples for EPR spectroscopic analysis of H_2O_2-activated DHP A(V59W). A 50 μM enzyme solution (final concentration) was reacted with a 10-fold excess of H_2O_2 in 100 mM KP_i (pH 7) at 25 °C. Variable reaction times (500 ms, 2 s, 30 s) were achieved by means of different aging lines. To make a sample, a standard 4 mm O.D. quartz EPR tube connected to a Teflon funnel was submersed in a liquid N_2-cooled isopentane bath at -110 °C. The reaction mixture was sprayed into the funnel, and the resulting frozen material was then packed at the bottom of the quartz tube using a packing rod fitted with a Teflon tip. The sample was then transferred to a liquid nitrogen storage Dewar for subsequent spectroscopic analysis. EPR spectra were recorded on an X-band (9 GHz) E-9 EPR spectrometer (Varian, El Palo, CA). A quartz finger Dewar insert was used to measure the EPR spectra at 77 K. The typical spectrometer settings were as follows: field sweep 200 G, scan rate 3.33 Gauss/s, modulation frequency 100 KHz, modulation amplitude 4.0 G, and microwave power 2 mW. The microwave frequency for each EPR experiment, typically close to 9.2977 GHz, was measured by an EIP-578 in-line microwave frequency counter (PhaseMatrix, San Jose, CA).

Resonance Raman spectroscopy. Protein samples used for resonance Raman experiments were expressed and purified as above and exchanged into 100 mM potassium phosphate buffer. The three Raman buffers at different pH were prepared from the same initial stock solutions to ensure that all the buffers contain the same compounds and no exogenous ligands were introduced. Thus, the results observed in the experiments are attributed to only the change in pH. The buffers used for the fluoride binding experiments were prepared from the same initial potassium phosphate solutions except that fluoride was intentionally introduced to a concentration of 20 mM.

The final protein concentration for all RR samples ~130 μM. The samples were placed into 5 mm diameter glass NMR tubes and stored on ice until used. Resonance Raman spectra were obtained by Soret band excitation using a Coherent Mira 900 titanium sapphire (Ti:sapphire) laser. The Ti:sapphire laser was pumped using a Coherent Verdi 10 frequency doubled diode pumped Nd:vanadate laser generating 10 W at 532 nm. The beam generated from the Ti:sapphire is tunable through approximately 700–1000 nm, and was sent through a Coherent 5–050 doubler to generate a normal working range of 400–430 nm for Soret band excitation. The beam was collimated and cylindrically focused to a vertical line of ~0.5 mm on the sample. Scattered light was collected with a Spex 1877 triple spectrometer (2400 grooves/mm final stage grating) equipped with an ISA SPEX liquid nitrogen-cooled CCD at ~1.7 cm^{-1} resolution. Computer acquisition of the data was accomplished with SpectraMax 2.0 software. The spectra were calibrated using known peaks from indene, toluene, and carbon tetrachloride standards.

Crystallization, structure determination and refinement: The DHP A(V59W) mutant protein was overexpressed in *E. coli Rosetta* (DE3 strain) cells, and purified by the procedures established for the purification of wt-DHPA (non-his tagged)[1]. The purified protein was in the ferric oxidation state of the heme iron, judging by the Soret maximum at 407 nm, and no further oxidation with $K_3Fe(CN)_6$ was deemed necessary.

All crystallizations were carried out at 4 °C using the hanging drop vapor diffusion method. Proteins were buffer exchanged into a 20 mM sodium cacodylate buffer (pH 5.9), and the protein solution, at the concentration of 8 mg/mL, was mixed with an equal volume of the crystallization solution and equilibrated against 600 μL of crystallization solution. The crystallization solution consisted of 0.2 M ammonium sulfate and PEG 4000 in the 30–36% (w/v) concentration range. Each protein crystallized in the presence of either 20 mM KF or buffer, and the crystals appeared after 3 days of incubation at 4 °C. The best diffraction quality crystals grew from 0.2 M ammonium sulfate and 32% PEG 4000. Crystals were harvested and soaked in mother liquor that was supplemented with 15% of PEG 400 as a cryoprotectant.

X-ray data were collected at Sector 22 (Southeast Regional Collaborative Access Team) of the Advanced Photon Source at Argonne National Laboratory. The diffraction data sets were reduced and scaled using *HKL-2000* suite [46] and belong to the $P2_12_12_1$ space group, same as wt-DHPA (metaquo), PDB 2QFK [47]. The DHP A(V59W) and DHP A(V59W-F) crystals diffracted to resolutions of 1.63 and 1.24 Å, respectively.

The structures of DHP A(V59W) in the presence and absence of NaF were determined by molecular replacement with *Phaser* [48] using the metaquo structure of wt-DHPA (PDB entry 2QFK) [47] as a search model. Cycles of the refinement and the map calculations were carried out with Refmac5 from *CCP4* suite of programs (Collaborative Computational Project, 1994) iterated with the model building using *Coot* [49]. V59W was refined to an R_{work} of 16.7% and R_{free} of 20.0%) and contained two protein molecules with 95.2% of residues in the most favored regions of the Ramachandran plot, with the remaining 4.8% in the additional allowed regions. V59W-F was refined to an R_{work} of 16.7% and

Table 1. Data collection and Refinement statistics.

	V59W	V59W-F
PDB code	3K3U	7MNH
Space group	$P2_12_12_1$	$P2_12_12_1$
Unit-cell parameters		
a (Å)	57.77	57.70
b (Å)	67.32	67.25
c (Å)	69.46	69.31
α (deg)	90.00	90.00
β (deg)	90.00	90.00
γ (deg)	90.00	90.00
Data collection		
Temperature (K)	100	100
Wavelength (Å)	1.54	1.12
Resolution (Å)[a]	30.29–1.63 (1.67–1.63)	48.26–1.24 (1.28–1.24)
Unique reflections	32461	71322
Completeness (%)[a]	98.9 (94.8)	97.5 (98.1)
R_{merge} (%)[b]	6.4 (17.1)	8.4 (55.0)
I/σ	12.4 (11.2)	21.4 (3.4)
Redundancy	4.2 (4.3)	4.5 (4.2)
Refinement		
R_{work}/R_{free} (%)[c]	16.7/20.0	16.7/18.7
Average B factor (Å^2)		
All atoms	11.33	9.44
No. of atoms		
Protein	2955	2730
Water	413	342
Rmsd from ideal		
Bond length (Å)	0.009	0.017
Bond angle (deg)	1.23	1.95
Ramachandran plot (%)		
Most favored	94.4	94.8
Allowed	5.6	5.2
Disallowed	0	0

[a]Values in parentheses are for the highest resolution shell. [b]Rmerge $\Sigma(|I-\bar{I}|/\Sigma I \times 100)$. [c]Rwork = $\Sigma|F_o-F_c|/\Sigma Fo \times 100$, where Fo is the observed structure factor amplitude and Fc is the calculated structure factor amplitude.

R_{free} of 18.7%) and contained two protein molecules with 94.8% of residues in the most favored regions of the Ramachandran plot, with the remaining 5.2% in the additional allowed regions. Data collection and refinement statistics are provided in Table 1.

Molecular dynamics simulations: Molecular dynamics (MD) simulations of the V59W mutant were conducted in order to observe the dynamics of the tryptophan in the distal pocket. The program NAMD was used to conduct the MD simulations [50]. The models were constructed based on the 2QFK X-ray crystal structure [47] using VMD's automated feature to add hydrogen atoms to the protein coordinates, soak the protein in a water box with periodic boundary conditions, and add ions (equivalent to 0.5 M NaCl) to create a neutral box. The *mutate residue* function was used to alter V59 to W. Three model calculations were conducted. The standard parameter set was used to study the dynamics of the V59W mutant. The V59W system consisted of 9254 water molecules, with 22 Na^+ and 20 Cl^- ions for charge neutralization, consistent with a charge of 2^- for the DHP A protein for the ferrous form. The periodic box parameters for this model were: X: 50.4 Å, Y: 57.2 Å and Z: 60.2. The second model consisted of ferric heme and tryptophan, V59WFN (where FN stands for ferric Fe and neutral Trp 59). The net charge on the DHP A protein in this model is -1, so that the number of ions is 22 Na^+ and 21 Cl^- required for charge neutralization of the solvent box. The periodic box lengths were: X: 60.2 Å, Y: 50.5 Å and Z: 61.1 with 9560 water molecules. MD simulations have been validated [51] using GROMACS [52, 53] as well as NAMD [54]. Ferric heme was parameterized based on charges obtained from density functional theory calculations (DFT) using DMol^3 [55-58].

RESULTS

Overexpression and purification of DHP A(V59W). Recombinant DHP A(V59W) was obtained by expression in *E. coli* and purified as previously described [42]. DHP A(V59W) was initially isolated as a mixture of the ferric [13, 47, 59] and oxyferrous [21, 47] forms, as typically seen for WT isoenzymes A and B, and subsequent treatment with an excess of potassium ferricyanide permitted the isolation of the ferric form. The optical purity ratio (Reinheitzahl or *R*z, defined as A_{Soret}/A_{280}) for DHP A(V59W) was found to be 3.4, lower than the literature values of ~4.1 for WT isoenzymes A and B [19, 42]. This was expected, however, as the V59W mutation increases the calculated A_{280} molar absorptivity coefficient to 18,450 $M^{-1}cm^{-1}$ in DHP A(V59W) from 12,950 $M^{-1}cm^{-1}$ in WT DHP A. At ~7 mg/L expression culture, the final yields of purified DHP A(V59W) protein were typically much lower that of WT DHP A (~35 mg/L), but still enabled sufficient protein to be obtained for performing the spectroscopic and structural studies detailed below.

Resonance Raman and UV-vis spectroscopic characterization of DHP A(V59W). The electronic absorption and resonance Raman (RR) spectra of DHP A(V59W) at pH 5, 6, and 7 are shown in Fig. 1. The electronic absorption spectrum of ferric DHP A(V59W) at pH 5 (Fig. 1(a),

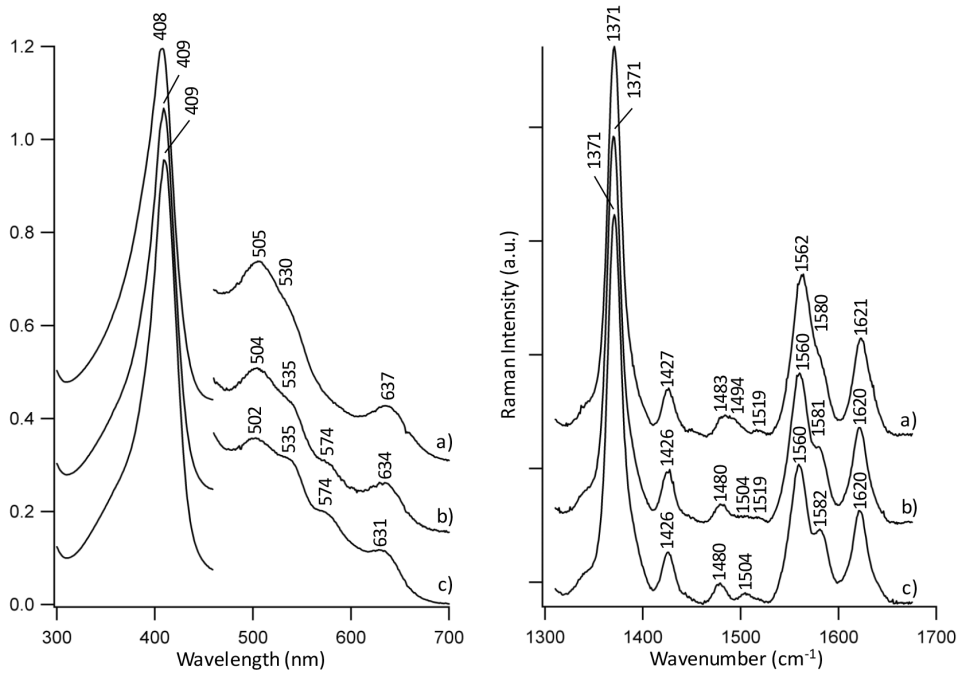

Fig. 1. Electronic absorption spectra (panel A) and RR spectra (panel B) of ferric DHP A(V59W) at (a) pH 5, (b) pH 6 and (c) pH 7 in 100 mM potassium phosphate buffer. The 460–700 nm region (panel A) has been multiplied by a factor of 5. Experimental conditions for panel B are: 406 nm excitation wavelength, 50 mW laser power at the sample, average of 6 spectra with 300 s integration time, 1.7 cm^{-1} spectral resolution. The intensities are normalized to that of the ν_4 band at 1371 cm^{-1}.

trace a) exhibits a Soret band at 408 nm, Q_1 and Q_0 bands at 505 and 530 nm, respectively, and a charge transfer (CT1) band at 637 nm, and is similar to the electronic absorption spectrum previously observed for WT-DHP A [UV-vis: 405 (Soret), 504, 538, 636 nm] at this pH [42]. Correlations based on studies of hemes a and a_3 in cytochrome *c* oxidase suggest that higher wavelengths for the CT1 band >645 nm correspond to 5-coordinate (5c) high-spin (HS) heme, whereas H_2O and F^- bound six coordinate (6c) HS forms are closer to 620 nm; these assignments have been supported by magnetic circular dichroism studies [60–63]. The slight differences between the V59W mutant and WT-DHP A are attributable to the presence of the distal cavity mutation. The resonance Raman spectrum of ferric DHP A(V59W) at pH 5 (Fig. 1(b), trace a) is nearly identical to WT-DHP A. The ν_4 mode is at 1371 cm^{-1}, typical of a ferric heme species, and the ν_3 mode shows a mixture of 5cHS and 6cHS species at 1494 and 1483 cm^{-1}, respectively, as expected in cases where ligation at the heme-Fe is mixed [64]. Effects of hydrogen bonding on 6cHS ligated species can be detected using the ν_3 mode as well [65, 66].

The electronic absorption spectrum of ferric DHP A(V59W) at pH 6 (Fig. 1(a), trace b) is consistent with the presence of a small amount of low spin (LS) species (574 nm). Compared to the pH 5 spectrum, the Soret band shifts to 409 nm, the Q_1 and Q_0 bands shift to 504 and 535 nm, respectively, and the CT1 band shifts to 634 nm. Accordingly, the RR spectrum of ferric DHP A(V59W) at pH 6 (Fig. 1(b), trace b) shows the presence of a small amount of 6cLS heme (ν_3 at 1504 cm^{-1}).

The electronic absorption spectrum of ferric DHP A(V59W) at pH 7 (Fig. 1(a), trace c) indicates an even greater amount of the low spin species (574 nm) with the Soret band at 409 nm, Q_1 and Q_0 bands at 502 and 535 nm, respectively, and the charge transfer band has shifted to 631 nm. The RR spectrum of ferric DHP A(V59W) at pH 7 (Fig. 1(b), trace c) also shows a greater population of 6-coordinate low spin heme (ν_3 at 1504 cm^{-1}). Moreover, the 5cHS component (ν_3 at 1494 cm^{-1}) initially present in the pH 5 spectrum is completely absent. Thus, the pH 5 spectrum is a mix of 5cHS and 6cHS species, the pH 6 spectrum is a mix weighted more heavily to 6cHS, and the pH 7 spectrum is 6cHS. The ν_3 mode for low spin DHP observed at 1504 cm^{-1} at pH 9.6 has been attributed to hydroxide binding [67]. The observed Raman spectra of the fluoride structures are compatible with this interpretation [68–70] if one considers replacement of F^- by OH^-. The absorption spectra for the F^-, OH^-, H_2O and 5-coordinate forms have been previously measured in DHP A. DHP-F and DHP-H_2O have CT1 maxima at 605 nm [71] and 636 nm [72], while DHP-OH lacks a CT1 band and has an absorption at 579 nm and 598 nm. However, these are bands are not observed until pH > 8, which was not studied here. Thus, the smaller shift from 636 nm to 631 nm shown in Fig. 1(a) is consistent with

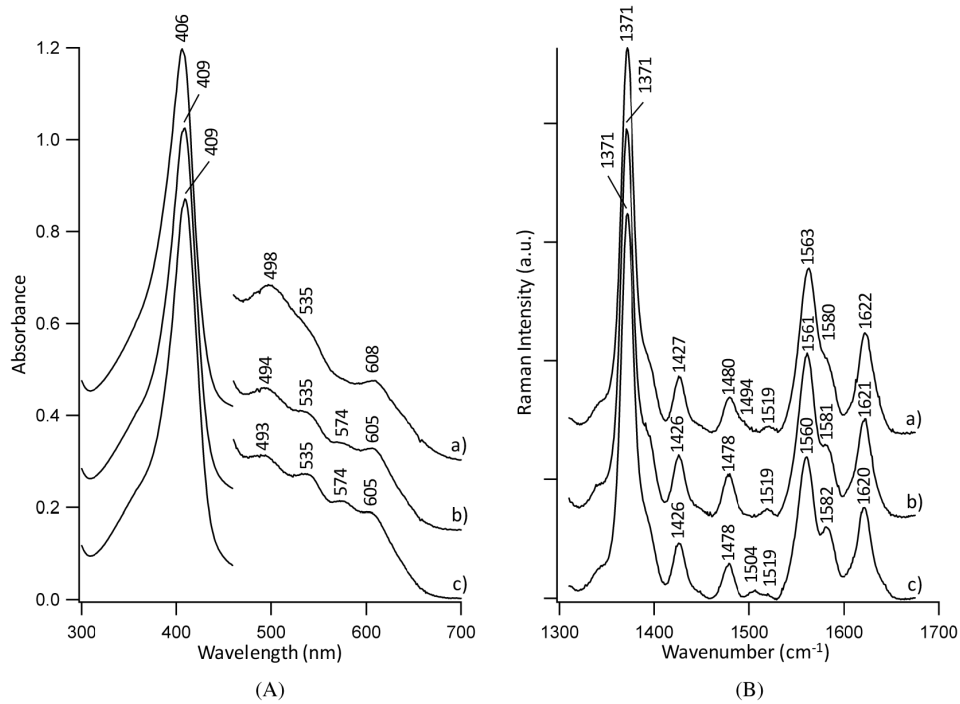

Fig. 2. Electronic absorption spectra (panel A) and RR spectra (panel B) of the ferric DHP A(V59W)-fluoride adduct at (a) pH 5, (b) pH 6 and (c) pH 7 in 100 mM potassium phosphate buffer containing 20 mM fluoride. The 460–700 nm region (panel A) has been multiplied by a factor of 5. Experimental conditions for panel B are: 406 nm excitation wavelength, 50 mW laser power at the sample, average of 6 spectra with 300 s integration time, 1.7 cm^{-1} spectral resolution. The intensities are normalized to the ν_4 band at 1371 cm^{-1}.

previous observed titration of the acid-alkaline transition (DHP-H_2O to DHP-OH) in DHP A [72] and the DHP-F form shown in Fig. 2(a) has a CT1 band in the region observed previously [71].

Analysis of the two ratios A_{Soret}/A_{380} and A_{614}/A_{645} demonstrates relative populations of 6-coordinate (6c) *vs*. 5c high spin (HS) heme present in hemoproteins. Generally, 5cHS heme species exhibit a slightly blue shifted and smaller extinction Soret band than their 6cHS counterparts, as well as a shoulder at 380 nm. As such, 5cHS hemes will yield a smaller A_{Soret}/A_{380} ratio than their 6cHS analogs. The A_{Soret}/A_{380} ratios for DHP(V59W) were found to be 1.95, 2.46, and 3.06 for pH 5, 6, and 7, respectively, and suggest a pH-dependent change in spin state from 5cHS at lower pH values to 6cHS under more basic conditions. Furthermore, the CT1 feature in a 5cHS heme is found at ~640 nm or higher, whereas that of a 6cHS heme is often closer to 630 nm. Thus, 5cHS hemes will yield a smaller A_{614}/A_{645} ratio than their 6cHS analogs, and is a complementary analysis to that of the A_{Soret}/A_{380} ratio for determining relative populations of heme coordination environments. The A_{614}/A_{645} ratios for DHP(V59W) were found to be 0.95, 1.20, and 1.45 for pH 5, 6, and 7, respectively, and are in agreement with the A_{Soret}/A_{380} ratio that suggests a pH-dependent change in spin state from 5c to 6c HS heme as the pH value is raised.

Resonance Raman and UV-vis spectra of DHP A(V59W) in the Presence of Fluoride Ion. Fluoride ion binding as a function of pH was employed to investigate if the introduction of the bulkier V59W mutation precludes substrate access to the heme active site [69]. The corresponding electronic absorption and resonance Raman spectra of DHP A(V59W) at pH 5, 6, and 7 in the presence of 20 mM NaF are shown in Fig. 2. The electronic absorption spectrum of ferric DHP A(V59W) at pH 5 with 20 mM fluoride (Fig. 2(a), trace a) is typical of a 6cHS ferric heme-F adduct with a Soret band at 406 nm, Q_1 and Q_0 bands at 498 and 535 nm, respectively, and the charge transfer band at 608 nm. The 30 nm blue-shifted CT1 band is commonly observed in heme proteins upon fluoride binding and subsequent formation of the 6cHS heme [71, 73]. The RR spectrum of ferric DHP A(V59W) at pH 5 with 20 mM fluoride (Fig. 2(b), trace a) is significantly different from the H_2O bound form (Fig. 1(b), trace a) because H_2O binding in the latter is an equilibrium mixture of 5cHS and 6cHS heme and conformational changes [12]. However, at pH 7 the spectra look similar with the puzzling exception of the CT1 band (Figs 1(a) and 2(a), trace c), suggesting that OH^- and F^- both may be in equilibrium as adducts to the heme-Fe under these conditions at pH 7.

The electronic absorption spectrum of ferric DHP A(V59W) [UV-vis: 409 (Soret), 494, 535, 608 nm] at

pH 6 with 20 mM fluoride (Fig. 2(a), trace b) again indicates the presence of a small amount of low spin species (574 nm), with an even greater amount of the low spin species observed at pH 7 [UV-vis: 409 (Soret), 493, 535, 574, 608 nm; Fig. 2(a), trace c]. The RR spectra of ferric DHP A(V59W) with 20 mM fluoride at pH 6 and 7 (Fig. 2(b), traces b and c, respectively) further corroborate of the presence of a 6-coordinate low spin heme (ν_3 at 1504 cm^{-1}) that increases with increasing pH. Moreover, the 5cHS heme component (1494 cm^{-1}) initially present in the pH 5 spectrum is completely absent at these higher pH values. The ν_4 mode is observed at 1371 cm^{-1} in all of the RR spectra and is indicative of a ferric heme. An oxyferrous adduct would be expected to have a lower value of 1368 cm^{-1} [74, 75], which is not observed in these experiments. In addition, there is a small band at 1519 cm^{-1} in a number of the spectra that we attribute to a photoreduction process that is observed despite the use of rapid spinning. Taken together, the results suggest that the heme-Fe remains accessible to fluoride ion binding, as also shown in the corresponding X-ray crystal structures, but also specific interactions of the tryptophan ring of W59 can affect the binding and even the pK_a of water bound to the heme Fe.

X-ray crystallography of DHP A(V59W) and its fluoride adduct. The X-ray crystal structures of the metaquo DHP A(V59W) mutant (PDB 3K3U) and the V59W mutant in complex with fluoride [denoted as DHP A(V59W-F)] (PDB 7MNH) are similar to that of the metaquo form of WT DHP A (PDB 2QFK [47]) (Fig. 3) with an overall RMSD of 0.36 Å for all 3 models as calculated with Chimera [76]. However, the distal pocket structure shows a significant local difference in that the steric bulk of the W59 residue forces the distal histidine, H55, to a solvent exposed conformation(s).

Despite its large size, the tryptophan shows a significant mobility in the distal pocket, with up to three conformations that can be fit to the electron density. In all conformations, the tryptophan is above and nearly parallel to the heme, blocking access to the heme-Fe although it is still not within van der Waal's interaction distance. The conformation(s) in the X-ray structure corresponds to pH 6. As discussed below, resonance Raman spectra and molecular dynamics simulations both suggested that the conformation of the tryptophan changes significantly between pH 6 and 7. Despite the mobility of W59, it occupies the space that normally would be taken up by a substrate. One mechanism of inhibition in DHP is the binding of molecules in the β-site perpendicular to the heme such that H_2O_2 binding and activation are no longer possible. This is supported by the observation that inhibitors such as 4-bromophenol preclude water binding to the heme iron (no 6cHS Fe-OH_2 adduct is observed), resulting in a 5cHS heme that can be observed by both UV-vis and RR spectroscopies [12, 77]. However, the flexibility of W59, in the mutant, could stabilize OH^- binding by hydrogen bonding to W59, blocking access of H_2O_2 and providing a mechanism of inhibition. The canonical inhibition mechanism in DHP involves binding of 4-bromophenol, which binds in the distal pocket, blocking access to the heme iron. In contrast to wild type DHP, attempts to co-crystallize a 4-bromophenol inhibitor with DHP A(V59W) resulted in little or ambiguous density (PDB 3O7N) that has been interpreted to suggest that 4-bromophenol (and similarly sized molecules like it) will not enter the distal pocket of DHP A(V59W). Indeed, no other substrate of DHP has been successfully co-crystallized with 4-bromophenol to-date suggesting that there is steric interference with W59. Instead of sterically blocking the heme iron, W59 stabilizes heme iron ligands, which may then compete with H_2O_2 binding.

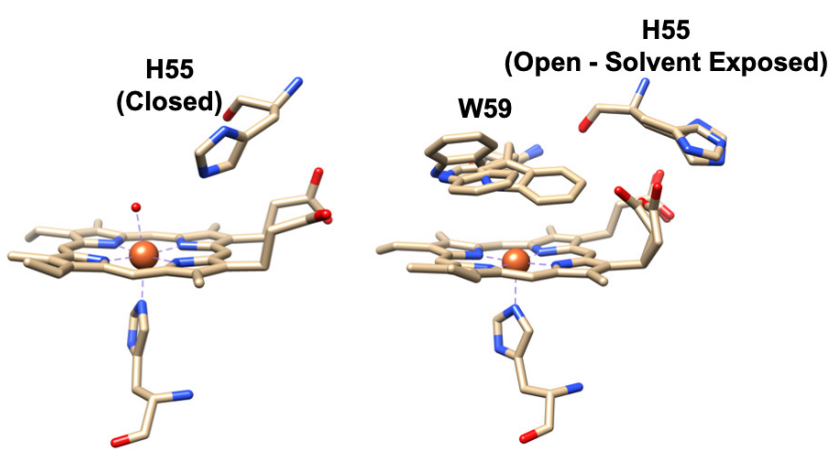

Fig. 3. Comparison of wild-type DHP A (2QFK; left) and DHP A(V59W) (3K3U; right) X-ray crystal structures. Both structures were obtained at 100 K. The distal histidine (H55) of wild-type DHP is shown in the closed position hydrogen-bonded to a water molecule. The V59W structure lacks the water molecule because all of the conformations of the W59 residue preclude binding of water.

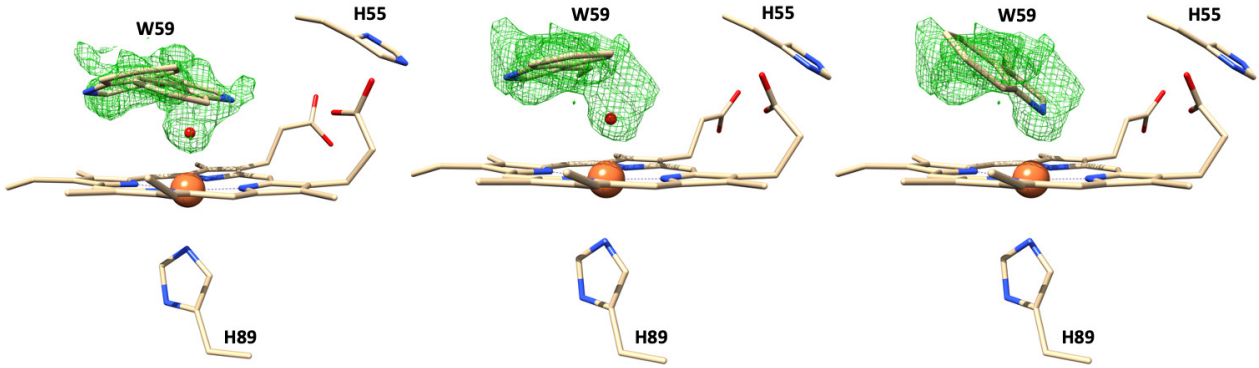

Fig. 4. Active site of both subunits of the crystallographic dimer. Difference densities are the $2F_o$-F_c maps calculated before addition of W59 to the coordinate file and are contoured at 3σ. The left panel of shows the difference electron density map above the heme of the first crystallographic subunit. The density can be fit with two conformations of W59, one similar to those observed in DHP A(V59W) (PDB 3K3U) where the W59 N can hydrogen bond to the heme bound ligand and one with W59 "flipped" with respect to those in V59W, both with an H_2O or F^- coordinated to the heme Fe. The center and right panels of show the difference electron density map above the heme of the second crystallographic subunit. The density can be fit two ways. The first is a conformation of W59 similar to DHP A(V59W) (PDB 3K3U) with an H_2O or F^- coordinated to the heme Fe (center). The second is a conformation of W59 that brings it into proximity of the heme-Fe (right).

The X-ray structure of the DHP A(V59W)-fluoride adduct is similar to the ferric structure, but the conformations of W59 in the distal pocket differ and only two are required to fit the observed density. Both active sites of the crystallographic dimer are shown in Fig. 4. The left panel of Fig. 4 shows the difference electron density map distal to the heme cofactor. Here, the density can be fit with two conformations of W59, one similar to that observed in V59W (PDB 3K3U) where the W59-$N^{\varepsilon 1}$ can hydrogen bond to the heme bound ligand, and one with W59 "flipped" with respect to those in V59W, both with an H_2O or F^- coordinated to the heme Fe. The center and right panels of Fig. 4 show the difference electron density map distal to the heme. This density can be fit two ways: 1) a conformation of W59 similar to V59W (PDB 3K3U) with a H_2O or F^- coordinated to the heme-Fe (Fig. 4: center) where the W59-$N^{\varepsilon 1}$ can hydrogen bond to the heme bound ligand, or 2) a conformation of W59 that brings it into proximity of the heme Fe (Fig. 4: right). This unusual conformation is only observed in the crystal treated with F^-, and the flexibility of W59 in the distal pocket makes modelling the density difficult. However, this raises an interesting question of whether or not W59-$N^{\varepsilon 1}$ can directly coordinate to the heme-Fe (ruled out below).

Enzymatic activity of DHP A(V59W) — The hydrogen peroxide-dependent oxidative dehalogenation of 2,4,6-trichlorophenol (TCP) as catalyzed by DHP A(V59W) at pH 6 is shown in Fig. 5.

The data at pH 7 are not shown because the reaction rate was too slow to measure [78]. The enzymatic reaction was initiated by the addition of H_2O_2, and the reaction was monitored using DCQ product formation [2,6-dichloro-1,4-benzoquinone (DFQ), λ_{max} = 275 nm].

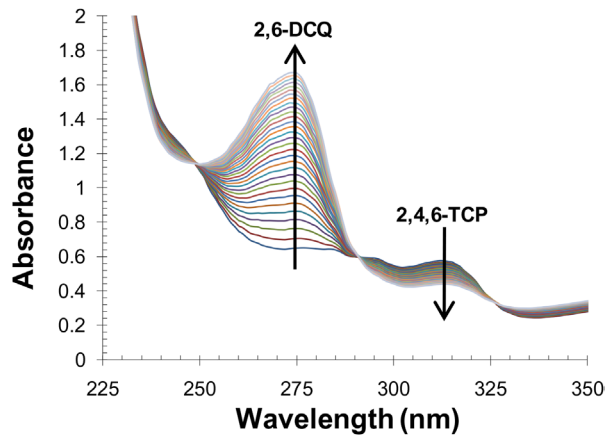

Fig. 5. Oxidative dehalogenation of 2,4,6-trichlorophenol (300 μM) as catalyzed by DHP A(V59W) (10 μM) and hydrogen peroxide (100 μM) at pH 7. The formation of 2,6-dichloroquinone was monitored at 275 nm.

In the absence of DHP A (non-enzymatic control), no product was observed under the conditions examined, in agreement with previous reports that showed a requirement for the enzyme [42, 45]. Under the conditions examined, the value of k_{cat} was determined to be ~0.18 s^{-1} for DHP A(V59W), or about 30% smaller than the value reported previously for WT DHP A [19]. At pH 7, this modest activity was essentially abolished.

To confirm the inability of the enzyme to be activated to a catalytically-competent form of DHP (*e.g.* Compounds I or ES) by H_2O_2 at pH 7, stopped-flow UV-vis spectroscopic studies were performed (Fig. 6).

Upon rapid mixing of a solution of DHP A(V59W) with a 10-fold excess of H_2O_2, no formation of a ferryl

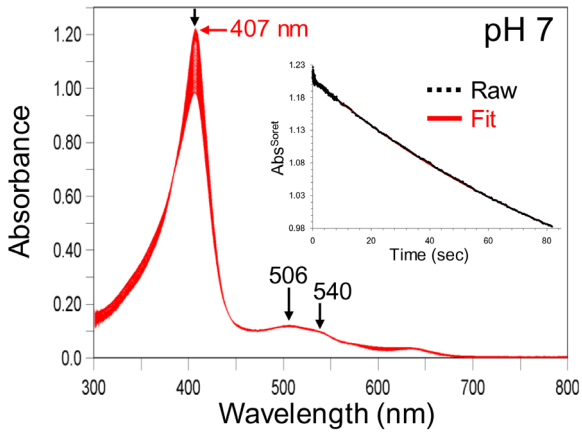

(a)

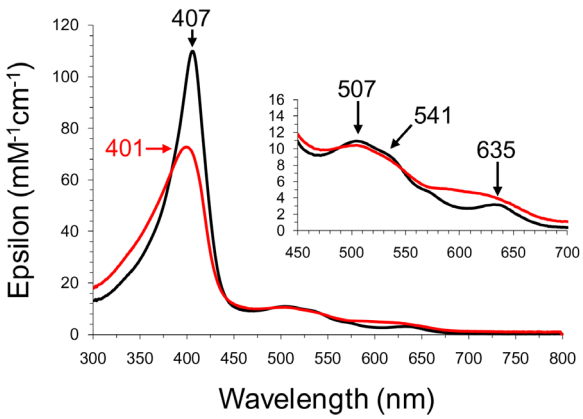

(b)

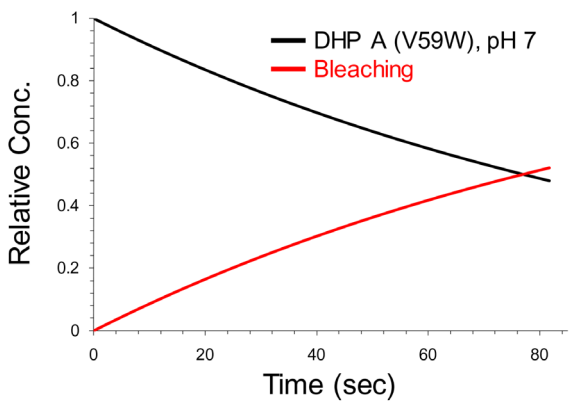

(c)

Fig. 6. Kinetic data for the reaction of DHP A(V59W) with hydrogen peroxide. (a) stopped-flow UV-vis spectra of the single-mixing reaction between DHP A(V59W) (10 μM) with a 10-fold excess of H_2O_2 at pH 7 (900 scans over 83 sec); inset - the single wavelength (407 nm) dependence on time obtained from the raw spectra and its fit with a superposition of the calculated spectral components. (b) calculated spectra of the two reaction components derived from the SVD analysis: ferric DHP A(V59W) (black) and the bleached product (red). (c) time dependences of the relative concentrations for the two components shown in the middle panel as determined from the fitting of the spectra in the top panel.

species was observed, in marked contrast to the observation of Compound ES under these conditions when employing WT DHP A [42]. Rather, a slow bleaching of the heme cofactor was noted over the course of the 85 s experiment, suggesting that the reaction of DHP A(V59W) does not proceed through the previously observable catalytic ferryl species noted for WT DHP A [42], and is therefore non-productive for substrate oxidation. To confirm that the lack of an observable Compound ES (Fe^{IV}=O + tyrosyl radical [32]) species was not due to endogenous reduction of the ferryl species by W59, EPR spectroscopy was performed on rapid-freeze-quench (RFQ)-trapped samples of the H_2O_2-activated DHP A(V59W). No signal was observed (data not shown), including the lack of the tyrosyl radical typically observed in DHP A [32], confirming no radical species (*e.g.* Tyr• or Trp•) were formed upon reaction of DHP A(V59W) with H_2O_2.

The marked difference in the activity of DHP A(V59W) as a function of pH can be interpreted as some form of stronger ligation to the heme-Fe by an exogenous axial ligand, consistent with the formation of a 6cHS complex as show in Fig. 1. The 6cHS heme ligand could be H_2O, but the evidence here supports deprotonated OH^- [67, 70, 72]. However, a simple binding of OH^- is not the origin of inhibition since it is well known that DHP can turnover catalytic substrates at pH > pK_a for the acid-alkaline phase transition, *i.e.* although hydroxide appears to be bound above pH 8.0, DHP is still peroxidase active [79]. Thus, the role played by the tryptophan is more subtle than an on-off switch due to steric bulk, but rather one related to stabilization of an axial ligand that is coordinated to the heme-Fe. In summary, the crystal structure of the V59W mutant shows a potentially significant interaction between the tilted tryptophan ring in the distal pocket and the heme-iron ligand (whether it be fluoride, hydroxide or water). Despite the enormous steric hindrance of the tryptophan, its dynamic nature in the distal pocket (as suggested by the multiple conformations of W59) results in an inhibition mechanism that is highly pH-dependent upon the strength of heme-Fe ligand binding.

Dynamics of the Trp-Heme-His adduct. As suggested above, dynamic motions of W59 in the distal pocket may be important for activity. Molecular dynamics simulations can provide an estimate of the time scales and probabilities for W59 motion among stable conformations. Figure 7 shows the two major conformations of W59 observed in the MD simulations. Figure 7(a) is taken from the neutral W59 ferrous heme MD simulation. Figure 7(b) is a representative structure from the MD simulation with anionic Trp59 and ferric heme parameters, with W59 perpendicular to the heme plane and ligated to the heme-Fe.

Figure 8 shows the Fe-(W59)N^{ε} distance plotted as a function of time in this model system. The simulation shows that Trp59 is observed in a bonding conformation for ~27 ns of the simulation, after which it dissociates

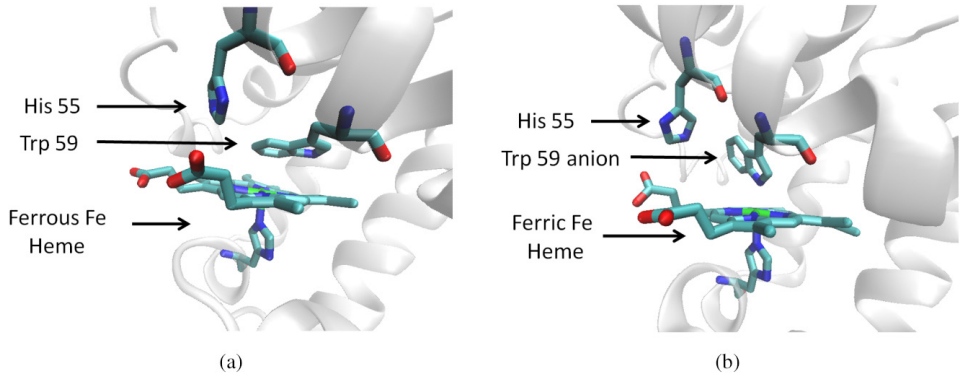

Fig. 7. Representations from molecular dynamics simulations of different oxidation states of heme Fe and charge states of Trp 59 of the DHP A(V59W) mutant are shown. (a) The neutral Trp 59 is nearly parallel to the heme plane of ferrous heme. (b) The anionic Trp 59 perpendicular to the heme plane and ligated to the heme of ferric heme.

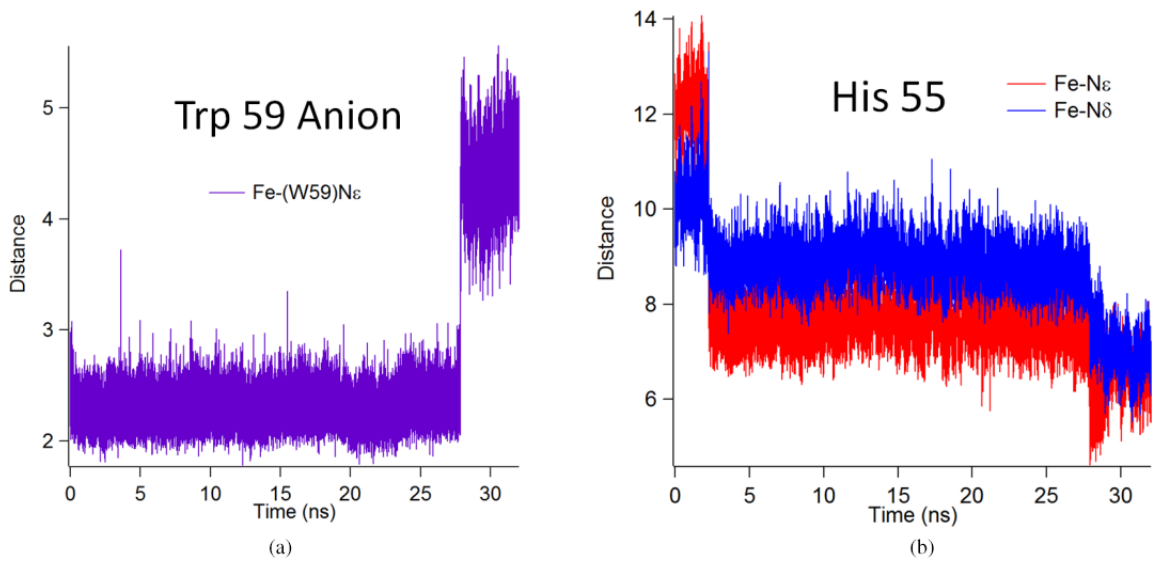

Fig. 8. Time courses from MD simulations of the ferric heme Fe and anionic Trp 59 form of the DHP A(V59W) mutant are shown. (a) The distance from the Fe atom to Trp 59 N^{ε} is shown. Trp 59 is observed in a bonding conformation for 27 ns of the simulation. However, it dissociates after 27 ns to a conformation similar to the neutral Trp 59 in Fig. 7(a). (b) The distance between the heme-Fe and the nitrogens of the distal histidine, His55, are shown.

and adopts a conformation similar to the neutral His. However, this model is artificial and without a strong interaction such as the Fe-N bond, W59 cannot maintain a geometry perpendicular to the heme plane. The formation of the Fe-N bond is not observed and the high pK_a of tryptophan practically ensures that it will not ligate to the heme. In summary, the MD simulations show that the parallel tryptophan conformation is dominant, but that the tryptophan and heme planes may deviate from parallel depending on the strength of the molecular interactions with ligands bound to the heme-Fe. The MD simulations also show a reasonable range of motion of the tryptophan that would permit enzymatic activity.

DISCUSSION

In designing the V59W mutant for DHP, the goals were similar to those for other globins where similar methods have been employed, namely, to block access to the heme-iron by increasing the steric bulk in the distal pocket and to observe accessible conformations of the tryptophan. In globins, the issue is accessibility of the Fe, which is clearly guarded by the appropriate set of amino acids above the heme in the distal pocket of SWMb and cloned human Mb [35, 80–83]. In a multi-functional peroxidase/peroxygenase, access to the Fe may affect catalytic efficiency or the conditions for switching between

different types of reactivity. Distal mutants have been studied in DHP [9, 14, 16, 28, 32, 84]. As the largest amino acid, tryptophan is a logical choice to use when one wants to investigate steric effects by site-directed mutagenesis [85, 86]. Tryptophan scanning mutagenesis locates regions of a protein where steric blockage can have a functional effect [87, 88]. Beyond sterics, tryptophan mutations can also be used to alter electron transfer pathways in heme peroxidases and monooxygenases: like tyrosine, tryptophan readily forms a neutral radical upon oxidation when it is located in the vicinity of the heme iron [32]. As such, both possibilities (sterics and alteration of electron transfer pathways) need to be considered. No such pathways were observed in the present work, which greatly simplified the understanding of the dynamic effects that already contained some subtlety.

While V59W presents a rather drastic change to the overall structure of the distal pocket, our previous studies with F21W suggested the feasibility of introducing this mutation into DHP [9, 16]. Moreover, the plasticity of the DHP distal pocket, which can accommodate large substrates such as 2,4,6-TCP [16], 5-Br-indole [89], and pentachlorophenol [22], also suggested that the active site would be able to accommodate such a change [90]. To visualize the results from various experiments and other heme proteins, it must be kept in mind that the heme cofactor is more deeply buried in the globin fold of DHP A, the distal histidine interacts strongly with the propionate side chains, and V59 is about 1.5 Å further from the heme than in SWMb [11]. This small difference in geometry likely turns out to have an important consequence for the structure of tryptophan mutation at that site: we describe a model of inhibition driven by hydrogen-bonding stabilization of the heme ligand. Studies in the presence of fluoride provide an additional probe of hydrogen-bonding in the distal pocket [91]. The simplest interpretation is that V59W is not involved in the catalytic reaction at pH 6 or lower and permits reactivity in equilibrium with the ligand binding. On the other hand, at pH 7, the tryptophan could polarize bound H_2O or F^-, which may lead both of them being substituted by OH^- and subsequent inhibition of DHP activity due to the stabilization of the resultant 6c adduct.

Multiple conformations of W59 in the DHP A distal pocket

The X-ray crystal structures reveal two general orientations of Trp59, both of which place the indole N^{e1} in range to hydrogen-bond with a sixth ligand to Fe (such as H_2O or F^-). As shown in Fig. 4, the orientation of the two significant W59 conformations make an angle of circa 45° with respect to the heme plane. Thus, it appears that the flexibility of W59 permits the indole side chain to hydrogen bond to heme-bound H_2O (or F^-), thereby stabilizing the binding of the ligand. The fact that the distal pocket can accommodate this bulky side chain is in agreement with numerous other observations of small molecule binding to DHP, including substrates 5-Br-indole [89], 2,4,6-TCP [16], 2,4-DCP [89], 4-NO_2-phenol [23], 4-Br-guaiacol [21], and pentachlorophenol [22], inhibitors such as 4-X-phenol (X = F, Cl, Br, I) [11, 12, 18], and azoles (benzotriazole, benzimidazole, imidazole, and indazole [20]) that bind to the heme or near the heme in the distal pocket, in addition to the previously crystallographically-characterized F21W mutant [9, 16]. One reason why DHP is able to accommodate such a broad number of substrates is the unusual flexibility of the distal histidine, which apparently permits the entry of large molecules, even when they are not ligated to the heme-Fe [8, 9, 21, 23, 90, 92]. However, it is surprising that W59 is able to adopt different conformations given that a tryptophan introduced by site-directed mutagenesis has restricted freedom of motion in the distal pocket due to its anchoring to the peptide backbone. One possible explanation is that, unlike other globins, DHP does not have a confined space or paths that lead to the oxygen-binding site: DHP has a relatively open architecture but must nonetheless respond to the binding of specific molecules in order to permit different oxidation mechanisms (peroxidase, peroxygenase, oxidase, oxygenase). The two or more different orientations of W59 in the distal cavity provide further evidence of a dynamic pocket and the importance of interactions with heme-bound H_2O as a crucial control mechanism [12, 93].

Reconciling the crystallographic and spectroscopic data

The resonance Raman spectrum shows that the equilibrium spin state of the heme-Fe shifts from a mixture of 5cHS/6cHS at pH 5 to mainly 6cHS at pH 7. The evidence for this is the change from a ν_3 band with two peaks at 1483 cm^{-1} and 1493 cm^{-1} at pH 5 to a single 6cHS peak at 1480 cm^{-1} at pH 7, and this structure is consistent with the loss of peroxidase enzymatic activity at the higher pH. Additionally, there a small band (<15% of the total intensity of the ν_3 band) at 1504 cm^{-1} at pH 7 that we believe can be assigned as a 6cLS OH^- ligated form.

The 6c heme structure at pH 7 as deduced from the UV-vis and resonance Raman spectroscopic data is significantly different than the X-ray crystal structure obtained at pH 5.9. The structural comparison with the X-ray crystal structure can only be made at pH 5.9, which is required for crystallization under the conditions identified in screens of DHP A and its mutants. The resonance Raman spectra of the DHP A(V59W)-F adduct show significant changes between pH 5 and 6, indicating that there may be a change of F^- ligation to the heme-Fe. There is also an apparent change in the 6cLS n_3 band from 1480 cm^{-1} to 1478 cm^{-1}, which may indicate a greater tendency to pull the Fe as pH increases. The pH 7 spectrum in Fig. 2(b) shows a small but significant change at pH 7 located in the band at 1519 cm^{-1}. This suggests

that even in the presence of fluoride, hydroxide is a competitive ligand (in equilibrium). W59 hydrogen-bonding interactions with both fluoride or H_2O show geometry and pH dependence. The X-ray crystal structure of DHP A(V59W) treated with fluoride also shows a conformation of W59 that makes an oblique angle with respect to the heme plane such that the indole-$N^{\varepsilon 1}$ is within van der Waal's contact with bound fluoride. The data suggest that a strong W59 interaction with heme-bound ligands, particularly F^-, dominates the energy landscape in the distal pocket and steric effects make relatively small energetic contributions.

Ruling out tryptophan ligation to the heme-Fe

Observation of the 6cLS heme-Fe at pH 7 is an interesting phenomenon, and the electron density shown in Fig. 4 allows one to model W59 within coordination proximity to the heme-Fe. Therefore, one cannot entirely rule out the possibility of ligation of the heme-Fe by W59 based on the electron density in the X-ray crystal structure alone. There are examples of mutations that change their conformation in order to ligate the heme-Fe. The mutation of distal valine (known as E9 in myoglobin, but also as V68, which is V59 in DHP) can produce a 6-coordinate adduct: namely, the V68E mutant in human Mb revealed that the negatively-charged glutamate was bound to the heme-Fe [33, 94]. Moreover, the pH-dependent nature of the transition from a 5cHS to a 6cHS heme does not require deprotonation of the tryptophan. Only the very small 6cLS Raman band at 1519 cm^{-1} could provide evidence, however such small populations of reduced protein are frequently observed in Raman studies due to photoreduction, and DHP's high reduction potential makes it especially prone to photoreduction [95, 96]. Further, multiple lines of evidence argue against a six-coordinate complex involving W59. First, the conformation of a heme-bound tryptophan would be strained (since it is restricted from being in an ideal perpendicular binding geometry as shown by the MD simulations, vide infra). Second, we are confronted by the fact that the pK_a of indole in aqueous solution is 16, and it is not immediately obvious what interaction in the distal pocket could cause a significant lowering in the pK_a of the tryptophan side chain (the distal pocket is largely hydrophobic and lacks strongly basic amino acid side chains that could play a role in modifying the pK_a of an internal amino acid). Known heme Fe ligands include histidine [47], cysteine [1, 97], methionine [98, 99], tyrosine [100], and aspartate [33, 94], but not tryptophan due to its high pK_a.

The steric effects were investigated by MD simulations. The precedence for 6cLS heme in DHP upon substrate binding can be found in X-ray crystal structures with azole compounds soaked into the distal pocket [20]. While the MD results show that the proximity of the tryptophan-N could lead to it coordinating the heme-Fe, the orientation of the second conformer of tryptophan is not ideal. Moreover, an interaction of the tryptophan with the heme-iron would require displacement of H_2O, OH^- or F^- to compete with direct ligation by tryptophan. To date there is no example of a tryptophan ligated to a heme iron in the PDB database. While the tryptophan does not directly ligate to the heme Fe, its polar imino (N-H) group appears to interact strongly with ligands bound to the heme-Fe, perturbing their equilibria mainly in a manner inhibitory to peroxidase activity.

CONCLUSION

We have prepared the V59W mutant of DHP A that introduces a bulky tryptophan residue into the distal pocket of this multifunctional catalytic globin. Not only does this mutation fold properly, it can be crystallized and studied as a function of pH to understand a unique role played by W59 in inhibiting DHP. W59 apparently has two major equilibrium conformations. The neutral indole form of W59 is parallel to the heme plane, with a second conformation in which W59 apparently interacts with a ligand bound to Fe (either H_2O or F^-) with the plane of the tryptophan making an angle of circa 45° with respect to the heme plane. The mutant can act as a peroxidase enzyme at pH 6, but not at pH 7. Using UV-vis and resonance Raman spectroscopies, we can infer that the reason is specific to the heme-iron being predominantly 6cHS at pH 7, which may result from a shift in the acid-alkaline transition of the heme-Fe, meaning that the Fe(III)-OH_2 is deprotonated so that the sixth ligand becomes hydroxide, as in Fe(III)-OH [72]. Hydroxide binds more strongly than fluoride so that this form dominates as supported by the resonance Raman data. Although MD calculations support the possibility of W59 binding directly to the heme iron, the high pK_a of the tryptophan side chain rules this out. There is still an electrostatic and protonation effect due to the tryptophan that gives rise to the hydroxide form at more than one pH unit lower than the pK_a of 8.1 observed for wild type DHP [72]. We find no evidence that tryptophan plays a role in the oxidation mechanism (*i.e.* radical formation), but instead the data reveal a new mechanism of DHP inhibition, namely an unusually strong H-bonding interaction between the tryptophan and the sixth axial heme ligand that inhibits enzyme activation by the co-substrate H_2O_2.

Acknowledgments

This project was funded by the National Science Foundation (CHE-1609446 and CHE-2002954). The authors would like to thank Drs. Vesna de Serrano and Michael Davis for their invaluable contributions. M.K.T. would like to acknowledge The University of Alabama start-up funds for support of this project.

REFERENCES

1. Sundaramoorthy M, Terner J and Poulos TL. *Structure* 1995; **3**: 1367–1378.
2. Poulos T, Edwards S, Wariishi H and Gold M. *J. Biologic. Chem.* 1993; **268 6**: 4429–4440.
3. Woodin SA, Lindsay SM and Lincoln DE. *Mar. Ecol-Prog. Ser.* 1997; **157**: 303–306.
4. Kevin TF, Sarah AW, Michael DW and David EL. *Marine Ecology Progress Series* 1999; **181**: 1–12.
5. Lincoln DE, Fielman KT, Marinelli RL and Woodin SA. *Biochem. Syst. Ecol.* 2005; **33**: 559–570.
6. Franzen S, Thompson MK and Ghiladi RA. *Biochim. Biophys. Acta* 2012; **1824**: 578–588.
7. Franzen S, Ghiladi RA, Lebioda L and Dawson J. Chapter 10 Multi-functional Hemoglobin Dehaloperoxidases, in: Heme Peroxidases, The Royal Society of Chemistry 2016, pp. 218–244.
8. Barrios DA, D'Antonio J, McCombs NL, Zhao J, Franzen S, Schmidt AC, Sombers LA and Ghiladi RA *J. Am. Chem. Soc.* 2014; **136**: 7914–7925.
9. Carey LM, Kim KB, McCombs NL, Swartz P, Kim C and Ghiladi RA. *J. Biol. Inorg. Chem.* 2018; **23**: 209–219.
10. McCombs NL, Smirnova T and Ghiladi RA. *Catal. Sci. Technol.* 2017; **7**: 3104–3118.
11. Lebioda L, LaCount MW, Zhang E, Chen YP, Han K, Whitton MM, Lincoln DE and Woodin SA. *Nature* 1999; **401**: 445.
12. Thompson MK, Davis MF, de Serrano V, Nicoletti FP, Howes BD, Smulevich G and Franzen S. *Biophys. J.* 2010; **99**: 1586–1595.
13. Zhao J, de Serrano V, Dumarieh R, Thompson M, Ghiladi RA and Franzen S. *J. Phys. Chem. B* 2012; **116**: 12065–12077.
14. Plummer A, Thompson MK and Franzen S. *Biochemistry* 2013; **52**: 2218–2227.
15. Sun S, Sono M, Du J and Dawson JH. *Biochemistry* 2014; **53**: 4956–4969.
16. Wang C, Lovelace LL, Sun S, Dawson JH and Lebioda L. *Biochemistry* 2013; **52**: 6203–6210.
17. Zhao J, de Serrano V, Le P and Franzen S. *Biochemistry* 2013; **52**: 2427–2439.
18. de Serrano V and Franzen S. *Biopolymers* 2012; **98**: 27–35.
19. D'Antonio J, D'Antonio EL, Thompson MK, Bowden EF, Franzen S, Smirnova T and Ghiladi RA. *Biochemistry* 2010; **49**: 6600–6616.
20. McCombs NL, Moreno-Chicano T, Carey LM, Franzen S, Hough MA and Ghiladi RA. *Biochemistry* 2017; **56**: 2294–2303.
21. McGuire AH, Carey LM, de Serrano V, Dali S and Ghiladi RA. *Biochemistry* 2018; **57**: 4455–4468.
22. Malewschik T, de Serrano V, McGuire AH and Ghiladi RA. *Arch. Biochem. Biophys.* 2019; **673**: 108079.
23. McCombs NL, D'Antonio J, Barrios DA, Carey LM and Ghiladi RA. *Biochemistry* 2016; **55**: 2465–2478.
24. Carey LM, Gavenko R, Svistunenko DA and Ghiladi RA. *Biochim. Biophys. Acta* 2018; **1866**: 230–241.
25. Malewschik T and Ghiladi RA. *Coord. Chem. Rev.* 2021; **441**: 213976.
26. Zhao J, Srajer V and Franzen S. *Biochemistry* 2013; **52**: 7943–7950.
27. Schkolnik G, Utesch T, Zhao J, Jiang S, Thompson MK, Mroginski MA, Hildebrandt P and Franzen S. *Biochem. Biophys. Res. Commun.* 2013; **430**: 1011–1015.
28. Jiang S, Wright I, Swartz P and Franzen S. *BBA-Proteins Proteom* 2013; **1834**: 2020–2029.
29. Zhao J, Rowe J, Franzen J, He C and Franzen S. *Biochem Biophys Res Commun* 2012; **420**: 733–737.
30. Poulos TL and Kraut J. *J. Biol. Chem.* 1980; **255**: 8199–8205.
31. Zhao J, de Serrano V and Franzen S. *Biochemistry* 2014; **53**: 2474–2482.
32. Dumarieh R, D'Antonio J, Deliz-Liang A, Smirnova T, Svistunenko DA and Ghiladi RA. *J. Biol. Chem.* 2013; **288**: 33470–33482.
33. Varadarajan R, Lambright DG and Boxer SG. *Biochemistry* 1989; **28**: 3771–3781.
34. Krzywda S, Murshudov GN, Brzozowski AM, Jaskolski M, Scott EE, Klizas SA, Gibson QH, Olson JS and Wilkinson AJ. *Biochemistry* 1998; **37**: 15896–15907.
35. Nienhaus K, Deng P, Olson JS, Warren JJ and Nienhaus GU. *J. Biol. Chem.* 2003; **278**: 42532–42544.
36. Nienhaus K, Deng P, Kriegl JM and Nienhaus GU. *Biochemistry* 2003; **42**: 9633–9646.
37. Quillin ML, Li T, Olson JS, Phillips Jr GN, Duo Y, Ikeda-Saito M, Regan R, Carlson M, Gibson QH, Li H and Elber R. *Journal of Molecular Biology* 1995; **245**: 416–436.
38. Brancaccio A, Cutruzzolá F, Allocatelli CT, Brunori M, Smerdon SJ, Wilkinson AJ, Dou Y, Keenan D, Ikeda-Saito M and Brantley RE. Jr. *J. Biol. Chem.* 1994; **269**: 13843–13853.
39. Ionascu D, Gruia F, Ye X, Yu A, Rosca F, Beck C, Demidov A, Olson JS and Champion PM. *J. Am. Chem. Soc.* 2005; **127**: 16921–16934.
40. Tomita T, Hirota S, Ogura T, Olson JS and Kitagawa T. *J. Phys. Chem. B* 1999; **103**: 7044–7054.
41. Petrich JW, Lambry JC, Balasubramanian S, Lambright DG, Boxer SG and Martin JL. *Journal of Molecular Biology* 1994; **238**: 437–444.
42. Feducia J, Dumarieh R, Gilvey LB, Smirnova T, Franzen S and Ghiladi RA. *Biochemistry* 2009; **48**: 995–1005.
43. Beers RF, Jr. and Sizer IW. *J. Biol. Chem.* 1952; **195**: 133–140.
44. Franzen S, Belyea J, Gilvey LB, Davis MF, Chaudhary CE, Sit TL and Lommel SA. *Biochemistry* 2006; **45**: 9085–9094.
45. Osborne RL, Taylor LO, Han KP, Ely B and Dawson JH. *Biochem. Biophys. Res. Commun.* 2004; **324**: 1194–1198.

46. Otwinowski Z and Minor W. Processing of X-ray diffraction data collected in oscillation mode, in: Carter CW, Jr. and Sweet RM. (Eds.) Methods in Enzymology, Academic Press, New York, 1997, pp. 307–326.
47. de Serrano V, Chen Z, Davis MF and Franzen S. *Acta Cryst.* 2007; **D63**: 1094–1101.
48. McCoy AJ, Grosse-Kunstleve RW, Adams PD, Winn MD, Storoni LC and Read RJ. *J. Appl. Crystallogr.* 2007; **40**: 658–674.
49. Emsley P, Lohkamp B, Scott WG and Cowtan K. *Acta Cryst.* 2010; **D66**: 486–501.
50. Phillips JC, Braun R, Wang W, Gumbart J, Tajkhorshid E, Villa E, Chipot C, Skeel RD, Kale L and Schulten K. *J. Comput. Chem.* 2005; **26**: 1781–1802.
51. Zhang Z, Santos AP, Zhou Q, Liang L, Wang Q, Wu T and Franzen S. *Biophysical Chemistry* 2016; **211**: 28–38.
52. Lindahl E, Hess B and van der Spoel D. *Molecular modeling annual* 2001; **7**: 306–317.
53. Van Der Spoel D, Lindahl E, Hess B, Groenhof G, Mark AE and Berendsen HJC. *J. Comput. Chem.* 2005; **26**: 1701–1718.
54. Phillips JC, Hardy DJ, Maia JDC, Stone JE, Ribeiro JV, Bernardi RC, Buch R, Fiorin G, Hénin J, Jiang W, McGreevy R, Melo MCR, Radak BK, Skeel RD, Singharoy A, Wang Y, Roux B, Aksimentiev A, Luthey-Schulten Z, Kalé LV, Schulten K, Chipot C and Tajkhorshid E. *J. Chem. Phys.* 2020; **153**: 044130.
55. Delley B. *J. Chem. Phys.* 1990; **92**: 508–517.
56. Delley B. *J. Chem. Phys.* 2000; **113**: 7756–7764.
57. Perdew JP and Wang Y. *Phys. Rev. B Condens. Matter* 1992; **45**: 13244–13249.
58. Franzen S. *J Am Chem Soc* 2001; **123**: 12578–12589.
59. D'Antonio EL, D'Antonio J, de Serrano V, Gracz H, Thompson MK, Ghiladi RA, Bowden EF and Franzen S. *Biochemistry* 2011; **50**: 9664–9680.
60. Roach MP, Pond AE, Thomas MR, Boxer SG and Dawson JH. *J. Am. Chem. Soc.* 1999; **121**: 12088–12093.
61. Pond AE, Sono M, Elenkova EA, McRee DE, Goodin DB, English AM and Dawson JH. *J. Inorg. Biochem.* 1999; **76**: 165–174.
62. Pond AE, Sono M, Elenkova EA, Goodin DB, English AM and Dawson JH. *Biospectroscopy* 1999; **5**: S42–S52.
63. Pond AE, Roach MP, Sono M, Rux AH, Franzen S, Hu R, Thomas MR, Wilks A, Dou Y, Ikeda-Saito M, Ortiz de Montellano PR, Woodruff WH, Boxer SG and Dawson JH. *Biochemistry* 1999; **38**: 7601–7608.
64. Callahan PM and Babcock GT. *Biochemistry* 1981; **20**: 952–958.
65. Mukai M, Nagano S, Tanaka M, Ishimori K, Morishima I, Ogura T, Watanabe Y and Kitagawa T. *J. Am. Chem. Soc.* 1997; **119**: 1758–1766.
66. Morikis D, Champion PM, Springer BA, Egebey KD and Sligar SG. *J. Biol. Chem.* 1990; **265**: 12143–12145.
67. Das TK, Franzen S, Pond A, Dawson JH and Rousseau DL. *Inorg. Chem.* 1999; **38**: 1952–1953.
68. Nicoletti FP, Droghetti E, Boechi L, Bonamore A, Sciamanna N, Estrin DA, Feis A, Boffi A and Smulevich G. *J. Am. Chem. Soc.* 2011; **133**: 20970–20980.
69. Droghetti E, Nicoletti FP, Bonamore A, Sciamanna N, Boffi A, Feis A and Smulevich G. *J. Inorg. Biochem.* 2011; **105**: 1338–1343.
70. Nicoletti FP, Thompson MK, Howes BD, Franzen S and Smulevich G. *Biochemistry* 2010; **49**: 1903–1912.
71. Zhao J, Moretto J, Le P and Franzen S. *J. Phys. Chem. B* 2015; **119**: 2827–2838.
72. Nienhaus K, Deng P, Belyea J, Franzen S and Nienhaus GU. *J. Phys. Chem. B* 2006; **110**: 13264–13276.
73. Smulevich G, Feis A and Howes BD. *Acc. Chem. Res.* 2005; **38**: 433–440.
74. Franzen S, Lambry JC, Bohn B, Poyart C and Martin JL. *Nature Structural Biology* 1994; **1**: 230–233.
75. Franzen S, Bohn B, Poyart C and Martin JL. *Biochemistry* 1995; **34**: 1224–1237.
76. Pettersen EF, Goddard TD, Huang CC, Couch GS, Greenblatt DM, Meng EC and Ferrin TE. *J. Comput. Chem.* 2004; **25**: 1605–1612.
77. Zhao J and Franzen S. *J. Phys. Chem. B* 2013; **117**: 8301–8309.
78. Ma H, Thompson MK, Gaff J and Franzen S. *J. Phys. Chem. B* 2010; **114**: 13823–13829.
79. Franzen S, Gilvey LB and Belyea JL. *Biochim. Biophys. Acta* 2007; **1774**: 121–130.
80. Olson JS, Soman J and Phillips Jr GN. *IUBMB Life* 2007; **59**: 552–562.
81. Balasubramanian S, Lambright DG and Boxer SG. *Proceedings of the National Academy of Sciences* 1993; **90**: 4718–4722.
82. Lambright DG, Balasubramanian S, Decatur SM and Boxer SG. *Biochemistry* 1994; **33**: 5518–5525.
83. Hubbard SR, Hendrickson WA, Lambright DG and Boxer SG. *Journal of Molecular Biology* 1990; **213**: 215–218.
84. Sun S, Sono M, Wang C, Du J, Lebioda L and Dawson JH. *Arch. Biochem. Biophys.* 2014; **545**: 108–115.
85. Baker P and Seah SYK. *J. Am. Chem. Soc.* 2012; **134**: 507–513.
86. Zhang X, Zhang Y, Yang G, Xie Y, Xu L, An J, Cui L and Feng Y. *Enzyme and Microbial Technology* 2016; **82**: 34–41.
87. Caballero-Rivera D, Cruz-Nieves OA, Oyola-Cintrón J, Torres-Nunez DA, Otero-Cruz JD and Lasalde-Dominicci JA. *Channels* 2012; **6**: 111–123.
88. Subbiah RN, Kondo M, Campbell TJ and Vandenberg JI. *The Journal of Physiology* 2005; **569**: 367–379.

89. Moreno-Chicano T, Ebrahim A, Axford D, Appleby MV, Beale JH, Chaplin AK, Duyvesteyn HME, Ghiladi RA, Owada S, Sherrell DA, Strange RW, Sugimoto H, Tono K, Worrall JAR, Owen RL and Hough MA. *IUCrJ* 2019; **6**: 1074–1085.
90. Chen Z, de Serrano V, Betts L and Franzen S. *Acta Cryst.* 2009; **D65**: 34–40.
91. Neri F, Kok D, Miller MA and Smulevich G. *Biochemistry* 1997; **36**: 8947–8953.
92. de Serrano VS, Davis MF, Gaff JF, Zhang Q, Chen Z, D'Antonio EL, Bowden EF, Rose R and Franzen S. *Acta Cryst.* 2010; **D66**: 770–782.
93. Thompson MK, Franzen S, Ghiladi RA, Reeder BJ and Svistunenko DA. *J. Am. Chem. Soc.* 2010; **132**: 17501–17510.
94. Varadarajan R, Zewert T, Gray H and Boxer S. *Science* 1989; **243**: 69–72.
95. D'Antonio EL, Chen TK, Turner AH, Santiago-Capeles L and Bowden EF. *Electrochemistry Communications* 2013; **26**: 67–70.
96. D'Antonio EL, Bowden EF and Franzen S. *J. Electroanal. Chem.* 2012; **668**: 37–43.
97. Poulos TL and Raag R. *FASEB J.* 1992; **6**: 674–679.
98. Rux JJ and Dawson JH. *FEBS Lett.* 1991; **290**: 49–51.
99. Arciero DM, Peng Q, Peterson J and Hooper AB. *FEBS Lett.* 1994; **342**: 217–220.
100. Adachi S-i, Nagano S, Ishimori K, Watanabe Y, Morishima I, Egawa T, Kitagawa T and Makino R. *Biochemistry* 1993; **32**: 241–252.